行政院國家科學委員會補助專題研究計畫□ 成 果 報 告 □X 期中進度報告

光電奈米材料與結構中激子之控制(2/3)

計畫類別：X 個別型計畫　　□ 整合型計畫
計畫編號：NSC 96-2628-M-009 -001 -MY3
執行期間： 96 年 08 月 01 日至 99 年 07 月 31 日

計畫主持人：謝文峰
共同主持人：程思誠
計畫參與人員：黃同慶、劉維仁、黃志賢、楊松、鄭信民、林國峰、邱偉豪、郭晉嘉、黃冠智、蔡智雅、林建輝、黎延垠。
成果報告類型(依經費核定清單規定繳交)：□精簡報告　X完整報告

本成果報告包括以下應繳交之附件：
□赴國外出差或研習心得報告一份
□赴大陸地區出差或研習心得報告一份
X出席國際學術會議心得報告及發表之論文各一份
□國際合作研究計畫國外研究報告書一份

處理方式：除產學合作研究計畫、提升產業技術及人才培育研究計畫、列管計畫及下列情形者外，得立即公開查詢
□涉及專利或其他智慧財產權，□一年■二年後可公開查詢

執行單位：國立交通大學光電工程研究所
中　華　民　國 98 年 5 月 22 日

表 Y04

行政院國家科學委員會專題研究計畫成果報告

光電奈米材料與結構中激子之控制(3/2)

Toward Control of Excitons in Photonic Nano-materials and Structures (3/2)

計畫編號：NSC 96-2628-M-009 -001 -MY3
執行期限：97 年 8 月 1 日至 98 年 7 月 31 日
主持人：謝文峰教授　　國立交通大學光電工程學系

一、中文摘要

我們成功地利用雷射濺鍍法長長高品質之氧化鋅磊晶薄膜在預度有奈米後的高 k 值Y_2O_3緩衝材之(111)矽基板上。以 X光繞射和穿透式電子顯微鏡我們決定ZnO 和 Y_2O_3之磊晶關係為(0001)< $2\bar{1}\bar{1}0$>ZnO||(111)<$10\bar{1}$>Y_2O_3。ZnO晶格是排列在Y_2O_3之六角形氧原子之子晶格上，而其界面結構可以用晶域匹配磊晶(domain matching epitaxy)模型來描述，也就是7個或8個ZnO {$11\bar{2}0$}面與Y_2O_3{$4\bar{4}0$}面的6或7晶格匹配；晶域匹配磊晶的結果導致大量地降低殘於應變。我們成長的ZnO薄膜即使只有0.21微米後從螢光光譜量測即顯示相當好的光學性質。

關鍵詞： II-VI 族半導體、寬能隙、氧化鋅、 磊晶薄膜、雷射濺鍍、氧化釔、晶體結構、晶域匹配磊晶、激子、 螢光光譜。

Abstract

High-quality ZnO epitaxial films have been grown by pulsed-laser deposition on Si (111) substrates using a nanothick high-*k* oxide Y_2O_3 buffer layer. Determined by X-ray diffraction and transmission electron microscopy, the epitaxial relationship between ZnO and Y_2O_3 follows (0001)< $2\bar{1}\bar{1}0$>ZnO||(111)<$10\bar{1}$>Y_2O_3. ZnO lattice aligns with the hexagonal O sublattice in Y_2O_3 and the interfacial structure can be well described by domain matching epitaxy with 7 or 8 ZnO {$11\bar{2}0$} planes matching 6 or 7 {$4\bar{4}0$} planes of Y_2O_3 and lead to a significant reduction of residual strain. Superior optical properties were obtained even for ZnO films as thin as 0.21 μm from photoluminescence results.

Keywords: II-VI semiconductor, wide band gap, ZnO, epitaxial film, pulsed-laser deposition, Y_2O_3, crystal structure, domain match epitaxy, exciton, photoluminescence.

二、緣由與目的

A ZnO-based II-VI semiconductor has been viewed as a promising candidate for developing UV/blue light emitting diodes (LEDs) and laser diodes in next generation because of its large direct band gap of 3.37 eV and exciton binding energy of 60 meV at room temperature (RT).[1] Because of low costs, excellent quality, large-area availability of Si wafer, and most importantly the unique opportunity of integrating wellestablished Si electronics with ZnO-based optoelectronic devices, many efforts have been put into growing high-quality ZnO on Si. Unfortunately, direct growth of epitaxial ZnO films on Si is a difficult task because of large diversity in lattice constants (15.4%) and thermal expansion coefficient (56%) as well as the formation of amphorous SiO2 layer at ZnO/Si interface.[2,3] Either polycrystalline or highly textured ZnO films were commonly obtained.[4] Although the growth of ZnO epilayers have

been achieved by adapting various nonoxide thin films, such as ZnS,[2] GaN,[3] and Mg/MgO,[5] as buffer layers, growing high-quality ZnO epi-films on Si is still regarded as an arduous challenge.

Epitaxial growth of insulator layers on Si is of great importance in achieving Si on insulator (SOI) structures and for the long-range goal of three-dimensional integrated circuits. Recently, Y_2O_3 has attracted great attentions because of its high dielectric constant, high conduction band offset, and thermodynamic stability with Si and is a promising candidate as an alternative gate dielectric.[6-8] Furthermore, the formation enthalpy of Y_2O_3 is larger in magnitude than that of SiO_2 and ZnO on thermal dynamics (ΔH_{Y2O3} = -1905.31 KJ/mol, ΔH_{SiO2} = -910.7 KJ/mol, and ΔH_{ZnO} = -350.5 KJ/mol).[3,9] This implies the formation of an amorphous silica layer can be obstructed during nucleation stage of Y_2O_3 on Si substrate and provides a nice template for subsequent epitaxial growth. Therefore, the growth of high-quality ZnO on Y_2O_3/Si offers very attractive potential to harmonically incorporate ZnO optoelectronic devices in silicon based integrated circuits. In this study, we report the growth of high-quality epitaxial ZnO films by pulsed-laser deposition (PLD) on a Y_2O_3/Si (111) composite substrate. The nanothick Y_2O_3 epi-layer serves not only as a buffer layer to ensure the growth of ZnO epi-film of high structural perfection but also as an insulator layer between ZnO and Si. The structural properties of the ZnO/Y_2O_3/Si(111) heteroepitaxial system was thoroughly examined by X-ray diffraction (XRD) and transmission electron microscopy (TEM). Superior optical characteristics of the ZnO film were verified by photoluminescence (PL) at room temperature (RT) and low temperature (LT).

三、研究方法與步驟

Si (111) wafers were cleaned by Radio Corporation of America (RCA) method and hydrogen passivated by a buffered hydrofluoric HF acid solution before being put into a multichamber MBE/electron-beam evaporation UHV system.[6] After heating to 700 °C, thin Y_2O_3 films were then deposited using electron beam evaporation from a high-purity Y_2O_3 source, with a cubic bixbyite structure of a = 10.606 Å, on the Si surface, with substrate temperatures maintaining at about 770 °C. The details of the growth and structure of Y_2O_3 were reported elsewhere.[7,10] The Y_2O_3/Si composite substrates were then transferred in air to the PLD growth system.[11] Prior ZnO deposition, Y_2O_3/Si (111) substrates were thermally treated at ~375 °C under UHV condition to clean the surface and to remove the moisture. A beam out of a KrF excimer laser (λ = 248 nm) at a repetition rate of 10 Hz was focused to produce an energy density ~ 5-7 J cm^{-2} on a commercial hot-pressed stoichiometric ZnO (5N) target. The ZnO layers were deposited at substrate temperature of 400 °C without oxygen flow; the growth rate is ~0.28 Å s^{-1}. XRD measurements were performed with a four-circle diffractometer at wiggler beamline BL17A of National Synchrotron Radiation Research Center, Taiwan with incident wavelength 1.3344 Å. Two pairs of slits located between the sample and the detector yielded a typical resolution of better than 4 × 10-3 Å-1. Cross-sectional TEM images were taken using a field-emission-gun type TEM (Philips TECNAI-20). The PL measurements were carried out using a He-Cd laser with wavelength of 325 nm as the pumping source. The light emission was dispersed by a Triax-320 spectrometer and detected by an UV-sensitive photomultiplier tube.

四、結果與討論

XRD radial scan (θ-2θ) along the surface normal of a 0.21μm thick sample is shown in Figure 1. The sharp peaks centered at 2.003 and 2.425 $Å^{-1}$ are Si (111) and ZnO (0002) reflections, respectively; the shoulder at 2.06 $Å^{-1}$ is attributed to Y_2O_3 (222) Bragg peak, revealing the cube-on-cube growth of Y_2O_3 on Si substrate. Additional oscillations observed in the radial scan are known as the thickness fringes, whose presence is an indication of sharp

interfaces and good crystalline quality of the grown film. From the fringes period, we derived the thickness of the Y_2O_3 buffer layer to be ~9.6 nm. The fact that only the (0002) reflection of ZnO appears, together with Y_2O_3 (222) and Si (111) reflections, in Figure 1 elucidates the grown ZnO layer is c-plane oriented. From ZnO (0002) peak width, we estimated the vertical coherence length about 0.20 μm indicating its structure maintains coherent almost over the entire film thickness. To examine the in-plane epitaxial relationship, we performed azimuthal cone scans (φ-scans) across the off-normal ZnO {101j1}, Y_2O_3 {440}, and Si {220} reflections, as illustrated in Figure 2. In contrast to ZnO grown directly on Si (111), where completely random in-plane orientation was observed, the presence of six evenly spaced ZnO {101j1} peaks confirmed the epitaxial growth of hexagonal ZnO film on the Y_2O_3/Si (111) substrate. The zone axis associated with the (0001) and (10$\bar{1}$1) reflections of ZnO is [$\bar{1}$2$\bar{1}$0], whereas the zone axis corresponding to Y_2O_3 (001) and (440) planes is [$\bar{1}$10]. The coincidence in angular positions of ZnO {10$\bar{1}$1} and Y_2O_3 {440} reflections, as shown in Figure 2, reveals these two zone axes are aligned with each other. With the crystal symmetry taken into account, we determined the inplane epitaixial relationship to be (2$\bar{1}$$\bar{1}$0)ZnO||(10$\bar{1}$)$Y_2O_3$. Furthermore, it is worth noticing that two sets of 3-fold symmetric peaks with 180° in-plane rotation from each other were observed in the Y2O3 {440} φ-scan, indicating the existence of two variants of Y_2O_3 on Si. The dominant one, B-type (111)-orientated domain with [2$\bar{1}$$\bar{1}$]$Y_2O_3$||[$\bar{2}$11]Si, has its axes rotated 180° about the surface normal from that of underlying Si and amounts over 86% in population; the minor one, A-type domain with [2$\bar{1}$$\bar{1}$]$Y_2O_3$||[2$\bar{1}$$\bar{1}$]Si, has the identical orientation as Si substrate.[7,12] Estimating from the line widths of radial and azimuthal scans across Y_2O_3 in-plane reflections, we obtained the average lateral domain size and twist angle of the ~9.6 nm thick Y_2O_3 buffer layer to be about 20.5 nm and 0.67°, respectively.

The lattice parameters of the ZnO layer are a= 3.258 Å and c = 5.182 Å as determined by fitting the positions of several Bragg reflections. As compared with the bulk values, a = 3.244 Å and c = 5.204 Å determined from a ZnO wafer, we found that the ZnO epitaxial film was tensily strained (0.45%) in the lateral direction and the lattice along the growth direction is correspondingly compressed by 0.42%. Cubic Y_2O_3 has a bixbyite structure, which can be described as a vacancy-ordered fluorite. Viewing along the [111] direction of Y_2O_3, the O sublattice in Y_2O_3 consists of two-dimensional defective hexagonal lattices stacking with ABC sequence along the [111] direction, as shown in Figure 3a, in which the filled circles denote O atoms and open circles represent O vacancies. The hexagonal unit cell has a lattice constant equal to a(Y_2O_3) $\cdot\sqrt{2}$ /4 = 3.750 Å and its axes are aligned with the (10$\bar{1}$$\bar{1}$)$Y_2O_3$directions, identical to the axes in ZnO basal plane. This elucidates the ZnO lattice is aligned with the O sublattice in Y_2O_3, as illustrated in Figure 3b, similar to the case of ZnO grown on c-plane sapphire.[13] The lattice mismatch between ZnO and O sublattices in Y_2O_3 and in sapphire are -13.5 and 18.1%, respectively. The opposite sign of lattice mismatch may explain the tensile and compressive strain observed in ZnO layers grown on Y_2O_3 and sapphire, respectively.

For systems with such a large lattice mismatch, the well established lattice matching epitaxy (LME), where films grow by one-to-one matching of lattice constants or pseudomorphically across the film-substrate interface, is not the favorable mechanism. Instead, domain matching epitaxy (DME),[13] where integral multiples of lattice planes containing densely packed rows are matched across the interface, provides a nice description of the interfacial structure of these systems. The planar spacing ratio of (11$\bar{2}$0)ZnO to parallel (4$\bar{4}$0)Y_2O_3, which coincides with the (11$\bar{2}$0) planes of O sublattice in Y_2O_3, 1.6292/1.875 falls between 6/7 and 7/8; this implies a matching of 7(8) planes of ZnO with 6(7) planes of Y2O3 across the interface along this direction. The large lattice mismatch is thus accommodated by the misfit dislocations localized at the interface with a periodicity of 6(7) times of (4$\bar{4}$0)Y_2O_3 interplanar spacing, leading to a significant reduction of residual strain down to ~1%. To verify this interfacial structure, we performed

cross-sectional TEM measurements. Figure 4a is the TEM micrograph along [11 $\bar{2}$]Si projection which shows atomically sharp ZnO/Y_2O_3 and Y_2O_3/Si interfaces; no intermediate reaction layer is observed in both interfaces. The periodic contrast variation along the ZnO/Y_2O_3 interface with an average spacing of ~1.2 nm found in the high resolution TEM images, shown in Figure 4(b), was attributed to the misfit dislocations induced strain field. The nearly periodically arranged extra (11 $\bar{2}$ 0)ZnO half-planes with a spacing of 6 or 7 (4 $\bar{4}$ 0)Y_2O_3 planes are clearly seen in the Fourier filtered image shown in Figure 4(c); this confirms the DME of ZnO on Y_2O_3 (111).

To further characterize the crystalline quality of the grown film, we measured θ-rocking curves and radial scans of ZnO normal reflections (000*n*) with *n*) 2 and 4 and in-plane reflections (*n*0 $\bar{n}$ 0) where *n*) 1, 2, and 3. Plotting the rocking curve width $\Delta\theta$ versus the diffraction order *n*, an analog to the Williamson and Hall plot, we obtained the tilt and twist angle of the film to be 0.27 and 0.52°, respectively. The line widths of the radial scans across ZnO surface reflections yield its lateral domain size of ~110 nm. It is interesting that the twist angle and domain size of the ZnO layer are significantly better than that of the Y_2O_3 buffer layer, 0.67° and 20.5 nm, even though we do see the ositive correlation between the structure perfection of buffer layer and that of the ZnO layer. Be aware that both the crystalline quality and optical properties of ZnO epi-layers are known to be significantly improved with increasing film thickness.[14] For a film as thin as 0.21 μm, the obtained tilt angle approaches that of ZnO epi-films of similar thickness grown on *c*-plane sapphire (0.05°) and its twist angle is even smaller than the latter films (0.58°),[11] demonstrating the high crystalline quality of the ZnO films grown on Y_2O_3.

We performed PL measurements at both 300 K (RT) and 13K (LT) to examine the optical performance of the 0.21 μm thick ZnO films. The RT-PL spectrum, shown in Figure 5a, exhibits a very weak deep-level emission (DLE) near 2.2 eV and a narrow near-band edge (NBE) emission at 3.296 eV, that is dominated by the free exciton emission. Both low DLE signals as well as the narrow and intense NBE emission are signatures of good optical performance. In comparison with the ZnO films grown on Si using other buffer layers such as LT-ZnO (NBE fwhm/film thickness: 130 meV/0.7 μm),15 ZnS (>100 meV/0.35 μm),2 and Mg/MgO (95 meV/1 μm),5 our ZnO film exhibits equally good or even better optical quality (100 meV/0.21 μm). Its performance is also comparable to ZnO films grown on *c*-plane sapphire (117 meV/0.4 μm)16 and CaF2 (~98 meV/1.3
μm).[17] Figure 5b illustrates the LT-PL spectrum and the enlarged spectrum of the NBE region together with the peak assignment is shown in the inset. The peak for NBE emission shifts to the
low energy side from LT to RT, shown in Figure 5, is due to the decrease in the band gap caused by the change of lattice constants or interaction with phonon.18,19 The dominant LT
luminescence line at 3.358 eV with a fwhm of ~9.1 meV and the lines around 3.368 eV were ascribed to the recombination of A-exciton bound to the neutral donors, D°2XA and D°1XA, respectively. By fitting the temperature-dependent intensity variation of the free A-exciton (FXA) line at 3.371 eV using the Arrhenius expression,[20] we obtained the binding energy of A-exciton 56.57 (6.53 meV, in good agreement with the 60 meV for bulk ZnO crystal. The other strong line at 3.329 eV (D°2XA)2e originates from the transitions involving radiative recombination of an exciton bound to a neutral donor (D°2XA) and leaving the donor in the excited state, also known as twoelectron satellite (TES). We made such assignment based on the ratio of donor binding energy to exciton binding energy ~0.34 as reported by Teke et al.[21] The FXA, D°2XA and TES emission accompanied with single phonon (FXA-1LO, D°2XA-1LO and TES-1LO) replica were observed at 3.301, 3.288, and 3.26 eV, respectively, and the peak at ~3.22 eV is the donor-acceptor pair (DAP) transition. These results demonstrated the superior optical properties of the ZnO thin film on Si using a Y_2O_3 buffer layer.

表 Y04

五、結論

High quality *c*-plane ZnO epitaxial films have been successfully grown by pulsed-laser deposition on Si (111) substrates with a thin Y_2O_3 buffer layer. Two (111) oriented domains with 180° in-plane rotation exist in the Y_2O_3 buffer layer and the B-type orientation domain prevails over the A-type one. The in-plane epitaxial relationship between the wurtzite ZnO and cubic Y_2O_3 follows $(2\bar{1}\,\bar{1}\,0)\mathrm{ZnO}\|(10\,\bar{1})\mathrm{Y_2O_3}$. The growth of ZnO on Y_2O_3 can be well described by domain matching epitaxy. The photoluminescence spectra of ZnO epi-films exhibit superior optical properties at room temperature even for films of thickness as thin as 0.21 μm. Our results demonstrate that the Y_2O_3 layer well serves as a template for integrating ZnO based optoelectronic devices with Si substrate.

六、自我評估

本年度計畫中我們進行兩部分光電物理之研究，分別為氧化(鎂)鋅薄膜與量子點之成長與光電性質研究和光子晶體波導之理論探討等。我們利用雷射濺鍍與 sol-gel 法成功地成長氧化(鎂)鋅薄膜與量子點等。成長之樣品我們分別研究，結構與應力、激子—聲子之交互作用、螢光、受激輻射與雷射現象、拉曼散射等等。在光子晶體量子電動力學研究方面，我們以分數微積分法首次成功地解釋光子晶體原子自發輻射動態行為與光譜。這一年來共發表 12 篇光電材料相關的 SCI 論文，即雷射動力學相關研究 SCI 論文計 3 篇，成果還算不錯。

七、參考文獻

(1) Tsukazaki, A.; Ohtomo, A.; Onuma, T.; Ohtani, M.; Makino, T.; Sumiya, M.; Ohtani, K.; Chichibu, S. F.; Fuke, S.; Segawa, Y.; Ohno, H.; Koinuma, H.; Kawasaki, M. *Nat. Mater.* **2005**, *4*, 42.

(2) Yoo, Y. Z.; Sekiguchi, T.; Chikyow, T.; Kawasaki, M.; Onuma, T.; Chichibu, S. F.; Song, J. H.; Koinuma, H. *Appl. Phys. Lett.* **2004**, *84*, 502.

(3) Nahhas, A.; Kim, H. K.; Blachere, J. *Appl. Phys. Lett.* **2001**, *78*, 1511.

(4) Cheng, H. M.; Hsu, H. C.; Yang, S.; Wu, C. Y.; Lee, Y. C.; Lin, L. J.; Hsieh, W. F. *Nanotechnology* **2005**, *16*, 2882.

(5) Wang, X. N.; Wang, Y.; Mei, Z. X.; Dong, J.; Zeng, Z. Q.; Yuan, H. T.; Zhang, T. C.; Du, X. L.; Jia, J. F.; Xue, Q. K.; Zhang, X. N.; Zhang, Z.; Li, Z. F.; Lu, W. *Appl. Phys. Lett.* **2007**, *90*, 151912.

(6) Hong, M.; Mannaerts, J. P.; Bowers, J. E.; Kwo, J.; Passlack, M.; Hwang, W.-Y.; Tu, L. W. *J. Cryst. Growth* **1997**, *175/176*, 422.

(7) Nieh, C. W.; Lee, Y. J.; Lee, W. C.; Yang, Z. K.; Kortan, A. R.; Hong, M.; Kwo, J.; Hsu, C.-H. *Appl. Phys. Lett.* **2008**, *92*, 061914.

(8) Kwo, J.; Hong, M.; Kortan, A. R.; Queeney, K. L.; Chabal, Y. J.; Mannaerts, J. P.; Boone, T.; Krajewski, J. J.; Sergent, A. M.; Rosamilia, J. M. *Appl. Phys. Lett.* **2000**, *77*, 130.

(9) Liang, J.-J.; Navrotsky, A.; Ludwig, T.; Seifert, H. J.; Aldinger, F. *J. Mater. Res.* **1999**, *14*, 1181.

(10) Lee, Y. J.; Lee, W. C.; Nieh, C. W.; Yang, Z. K.; Kortan, A. R.; Hong, M.; Kwo, J.; Hsu, C.-H. *J. Vac. Sci. Technol., B* **2008**, *26*, 1124.

(11) Liu, W.-R.; Hsieh, W. F.; Hsu, C.-H.; Liang Keng, S.; Chien, F. S.-S. *J. Appl. Crystallogr.* **2007**, *40*, 924.

(12) Tung, R. T.; Bean, J. C.; Gibson, J. M.; Poate, J. M.; Jacobson, D. C. *Appl. Phys. Lett.* **1982**, *40*, 684.

(13) Naraya, J.; Larson, B. C. *J. Appl. Phys.* **2003**, *93*, 278.

(14) Shim, E. S.; Kang, H. S.; Kang, J. S.; Kim, J. H.; Lee, S. Y. *Appl. Surf. Sci.* **2002**, *186*, 474.

(15) Xiu, F. X.; Yang, Z.; Zhao, D. T.; Liu, J. L.; Alim, K. A.; Balandin, A. A.; Itkis, M. E.; Haddon, R. C. *J. Cryst. Growth* **2006**, *286*, 61.

表 Y04

(16) Chen, Y. F.; Bagnall, D. M.; Koh, H. J.; Park, K. T.; Hiraga, K.; Zhu, Z.; Yao, T. *J. Appl. Phys.* **1998**, *84*, 3912.

(17) Ko, H. J.; Chen, Y. F.; Zhu, Z.; Yao, T. *Appl. Phys. Lett.* **2000**, *76*, 1905.

(18) Hsu, H. C.; Cheng, C. S.; Chang, C. C.; Yang, S.; Chang, C. S.; Hsieh, W. F. *Nanotechnology* **2005**, *16*, 297.

(19) Wang, Lijun; Giles, N. C. *J. Appl. Phys.* **2003**, *94*, 973.

(20) Jiang, D. S.; Jung, H.; Ploog, K. *J. Appl. Phys.* **1988**, *64*, 1371.

(21) Teke, A.; O¨ zgu¨r, U¨ .; Dogan, S.; Gu, X.; Morkoc¸, H.; Nemeth, B.; Nause, J.; Everitt, H. O. *Phys. ReV. B* **2004**, *70*, 195207.

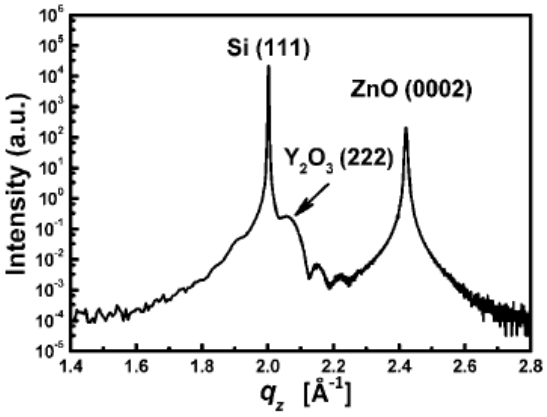

Figure 1. XRD radical scan along surface normal.

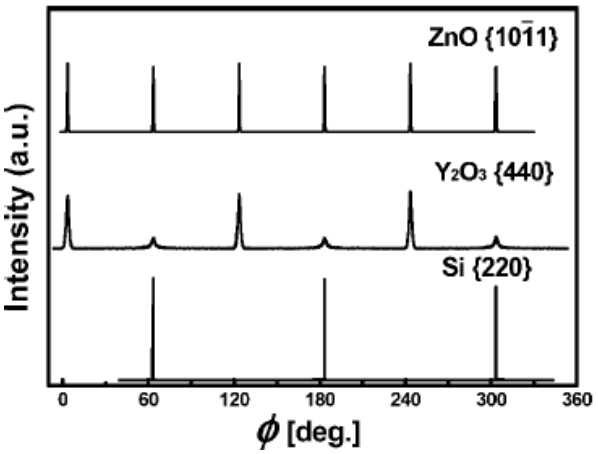

Figure 2. ϕ-scan profiles across $\{10\bar{1}1\}_{ZnO}$, $\{440\}_{Y_2O_3}$, and $\{220\}_{Si}$ off-normal reflections.

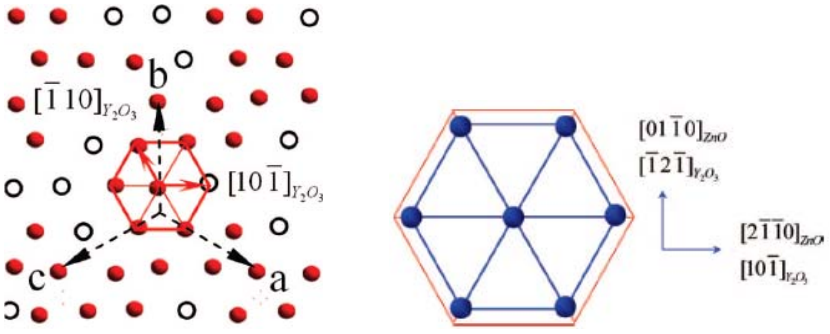

Figure 3. (a) Schematic of atomic arrangement of O sublattice in Y_2O_3 (111) planes, where the filled circles are O atoms and the open circles denote O vacnacies. The dashed arrows are (111) projection of the basis vectors of Y_2O_3 cubic lattice. (b) Illustration of the lattice alignment of ZnO basal plane (small hexagon) with O sublattice in Y_2O_3 (large hexagon).

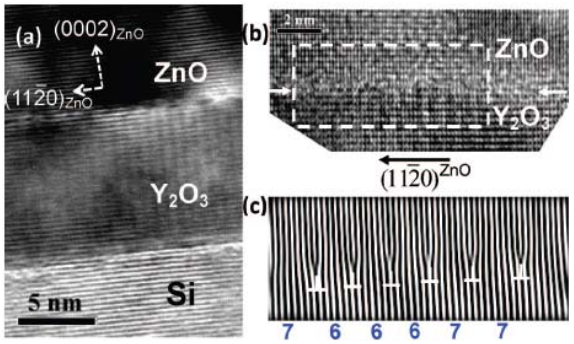

Figure 4. (a) Cross-sectional TEM micrograph recorded along $[11\bar{2}]_{Si}$ projection. The high resolution image of the ZnO/Y_2O_3 interface is shown in (b). The Fourier filtered image of the area enclosed by the dashed rectangle in (b) is displayed in (c), on which the number of $(\bar{4}\bar{4}0)_{Y_2O_3}$planes between adjacent extra $(11\bar{2}0)_{ZnO}$ half-planes are marked below.

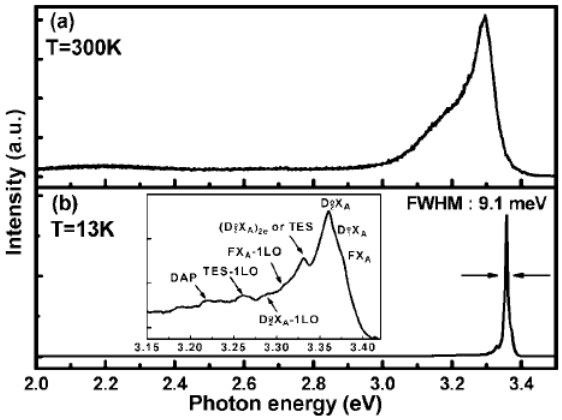

Figure 5. PL spectra of the ZnO film on Y_2O_3/Si (111) measured at (a) 300 and (b) 13 K. The inset is the extended spectrum of NBE emission in (b).